metals

Article

Emulsification and Flow Characteristics in Copper Oxygen-Rich Side-Blown Bath Smelting Process

Xiaolong Li [1,2], Yan Liu [1,2], Dongxing Wang [3] and Tingan Zhang [1,2,*]

1 Key Laboratory for Ecological Metallurgy of Multimetallic Mineral, Ministry of Education, Shenyang 110819, China; 1410283@stu.neu.edu.cn (X.L.); liuyan@smm.neu.edu.cn (Y.L.)
2 School of Metallurgy, Northeastern University, Shenyang 110819, China
3 Guangdong Research Institute of Rare Metals, Guangzhou 510650, China; wangdongxing@irmgdas.gd.cn
* Correspondence: zhangta@smm.neu.edu.cn; Tel.: +86-138-4020-5331

Received: 15 September 2020; Accepted: 14 November 2020; Published: 17 November 2020

Abstract: Oxygen-rich side-blown bath smelting (OSBS) is a kind of copper smelting technology with high efficiency, energy-saving, and environment-friendly characteristics. However, emulsification and flow pattern as significant hydrodynamic parameters have been rarely studied for the OSBS process. The formation, size distribution of slag-matte droplets, and flow patterns of the melt in the industry were physically simulated and investigated by the water–oil system in this paper. Moreover, a mathematical model was proposed to estimate the interfacial area between the liquid slag and the emulsion droplets. The results reveal that the typical droplet diameter is in the range of 2 mm to 4 mm. The increase in gas velocity leads to decreasing droplet size and increasing the interfacial area. However, the increase of the injection angle tends to generate large droplets, which is not conducive to strengthen the OSBS process. The correlations of average diameter with Weber number are analyzed in the emulsified region. Besides, the flow patterns in the OSBS process can be divided into the chaotic zone and the quiet zone. In the industrial OSBS process, suitable gas velocity and a small injection angle will refine the copper matte droplets and accelerate the smelting process.

Keywords: emulsification; size distribution; interfacial area; weber number; flow pattern; physical modeling

1. Introduction

Copper and its alloys are widely used in the fields of electric power, construction, machinery, transportation, and electronics due to easy processing, corrosion resistance, and excellent thermal and electrical conductivity. In 2017, global refined copper production reached 23.5 million tons [1]. The higher environmental standards and resource efficiency promote the renewal and development of copper smelting technology. Among these advanced technologies, the oxygen-rich side-blown bath smelting (OSBS) technology derived from the Vanyukov process has been gradually applied in the metallurgical processes, such as the smelting process of copper concentrate [2], the reduction of high lead slag [3], and even the extraction of gold from minerals.

Multiphase fluid flow plays a significant role in bath smelting processes, such as homogenizing the melt, enhancing the rates of oxidizing reactions, and promoting interphase interactions [4]. Many investigations on flow patterns and mixing performance of the top and bottom smelting processes have been found [5–12], but few on the side-blown smelting process [13–15]. For instance, the flow patterns in the top-blowing smelting process could be divided into five zones: Impact zone, circulation zone, splashing zone, fluctuation zone, and quiet zone [5–7]. Nevertheless, the bottom-blowing bath was divided into four kinds of zones: Bath zone, fountain zone, gas zone, and oscillation zone [8]. Different flow regimes would affect the size, rising velocity, and dispersion of the bubbles, directly affecting the reaction rate and oxygen utilization [9,10]. Moreover, Shui et al. studied the mixing phenomena in water [11] and oil-water [12] systems agitated by the gas from the bottom and found that the mixing time decreased with increasing the gas flow rate [12]. Zhao et al. [6] and Sahai et al. [13] also found that the mixing time decreased obviously when increasing the gas-liquid contact area. However, the high gas flow rate would enhance the fluctuation and splashing of liquid in the bath. Compared with the top and bottom smelting process, the side-blowing system showed a better mixing efficiency [14]. The side blowing in the jetting regime would provide deeper penetration and longer gas jet trajectory than other cases [15]. Thus, investigations on the flow patterns of the OSBS process are essential to reveal fluid flow and more fluid dynamics information.

For all bath smelting systems, the emulsification is of importance in creating a large interfacial area between the liquid slag and the molten metal, accelerating mass transfer rates, and chemical reaction processes [16]. The size distribution, surface area, flow behaviors, and residence time of the emulsified droplets are essential to the mass transfers of metals and the intensification of the smelting process [17–26]. For example, the formation and the size distribution of the emulsified droplets were investigated by water modeling and high-temperature studies. Khajavi et al. [17] investigated the formation of the water–oil emulsified droplets and found that the size of the emulsified droplets was controlled by the shear force and the surface energy. The droplets became smaller at a higher gas flow rate and eventually became stable at a specific size. Koch et al. [18] carried out the hot model experiments on the decarburization of Fe-C melts and verified that the formation of metal droplets enhanced the rate of decarburization. However, the formation of the dispersed droplets was caused by the splashing of the melt, which showed different results. The formation of the metal emulsion was analyzed by Song et al. [19] in the lead–salt system. A bubble dome with a metal film was formed first and after that, metal droplets formed when the bubble become detached from the interface. While the size of the metal emulsion was below 100 μm. To quantify the interfacial area between the emulsion droplets and the liquid slag, a mathematical model was obtained to estimate the interfacial area but without specific data [17]. Martín et al. [20] measured the mass transfer coefficient ($K_L A$) in a water-vaseline emulsified system. Whereas the interfacial area was not measured. Although the interface area was unclear, Lin et al. [21] proposed a generalized model to evaluate the transitional volume of droplets entrained in the metallurgical emulsions. Akdogan et al. [22] investigated the holdup distribution of the emulsified droplets, which was correlated by using the modified Froude number. Besides, the residence time distribution of emulsified droplets of different sizes in the emulsion region was studied [23–26] and several mathematical models for the prediction of the residence time of the emulsified droplets have been developed [24–26].

To sum up, the formation, the size distribution, and the flow characteristics of the emulsified droplets are quite different due to the various smelting systems, physical properties of the melts, and even operating conditions. The calculation of the interfacial area between metal droplets and liquid slag is still difficult. More importantly, these important hydrodynamic parameters are scarce for the OSBS process.

In the present study, a lab-scale OSBS physical model was set up. The emulsifying phenomena and flow characteristics under different gas velocities and injection angles were investigated by the physical model. Moreover, a mathematical model was proposed to estimate the interfacial area between the liquid slag and the emulsion droplets. Some suggestions on how to strengthen the industrial OSBS process were also given.

2. Experimental Methods

2.1. Physical Modeling

In the industrial OSBS process, copper concentrate, flux, and fuel are added from the top of the furnace and melt into the liquid phase. Oxygen-rich air is pumped into the furnace through the immersed tuyere on both sides of the furnace. The oxygen-rich air agitates the melt violently, forming the emulsion droplets and accelerating the slagging reactions and matting smelting. The geometric structures, physical properties of the melt, and operating conditions of the industrial OSBS process are clearly shown in Table 1. To simulate and investigate the phenomena of emulsification and flow behaviors, the OSBS physical model is established.

Table 1. Dimensions and main parameters of the OSBS furnace and physical model.

Parameters	OSBS Furnace (Prototype)	Physical Model
Furnace size (m)	11.93 (Length) × 2.20 (Width) × 6.82 (Height)	1.490 (Length) × 0.275 (Width) × 0.852 (Height)
Smelting area (m^2)	18	0.281
Liquid density (kg/m^3)	4500 (Matte); 3400 (Liquid slag)	998 (Water); 890 (Oil)
Gas density (kg/m^3)	1.187 (Oxygen-rich air)	1.146 (Air)
Gas flow rate (Nm^3/s)	1.83~2.71	4.86×10^{-3}~7.17×10^{-3}
Number of nozzles	10	10
Nozzle diameter (m)	0.03	0.00375
Injection angle (°)	7~12	7,12,17
Interface tension (N/m)	0.02~0.06 (Matte-liquid slag)	0.024 (Water-oil)

According to the theory of models, two processes may be considered completely similar if they take place in a similar geometrical space and if all dimensionless numbers necessary to describe them have the same numerical value [27]. To ensure the geometric similarity, a 1/8 scaled-down water model was constructed proportionally with the industrial OSBS furnace in this paper. A schematic diagram of the experimental setup is clearly shown in Figure 1. For the dynamic similarity, it is impossible to keep all dimensionless numbers constant in reactors of different sizes due to the complex physical transfer processes in the OSBS process. However, it is feasible to maintain the dominant dimensionless number equal in the OSBS furnaces of different sizes. The inertia force of fluids, the gravity of liquid slag, and the buoyancy of gas are essential factors for the multiphase flow in the OSBS process [28]. Therefore, the modified Froude number (Fr′) [28–30] is kept constant between the prototype (industrial reactor) and the model (physical model). The modified Froude number is expressed as:

$$Fr_{\mathrm{m}}{}' = Fr_{\mathrm{p}}{}' = \frac{\rho_{\mathrm{g,m}}}{\rho_{\mathrm{l,m}}}\frac{U_{\mathrm{m}}^2}{gd_{\mathrm{m}}} = \frac{\rho_{\mathrm{g,p}}}{\rho_{\mathrm{l,p}}}\frac{U_{\mathrm{p}}^2}{gd_{\mathrm{p}}} \tag{1}$$

where U is the gas velocity (m/s), d is the nozzle diameter (m), ρ_g is the gas density (kg/m^3), ρ_l is the liquid density (kg/m^3), p represents the prototype parameters, and m represents the model parameters.

Gas velocity U is calculated as:

$$U = \frac{4Q}{\pi d^2} \tag{2}$$

where Q is the gas flow rate (m^3/s).

Combining with the Equations (1) and (2), Equation (3) is obtained to calculate the gas flow rate in the physical model based on the values of the industrial OSBS furnace shown in Table 1.

$$Q_{\mathrm{m}} = Q_{\mathrm{p}} \times \left(\frac{\rho_{\mathrm{g,p}}}{\rho_{\mathrm{g,m}}}\right)^{0.5} \times \left(\frac{\rho_{\mathrm{l,m}}}{\rho_{\mathrm{l,p}}}\right)^{0.5} \times \left(\frac{d_{\mathrm{m}}}{d_{\mathrm{p}}}\right)^{2.5} = 2.646 \times 10^{-3} Q_{\mathrm{p}} \tag{3}$$

Besides, the interface tension of the water–oil system (in the physical model) should also be equal to that of the matte-liquid slag system (in the industrial process) to acquire similar emulsified phenomena. Therefore, the specific oil was selected to simulate the copper slag phase in the industry, as shown in Table 1. Dimensions and main parameters of the industrial furnace and the physical model are also shown in Table 1.

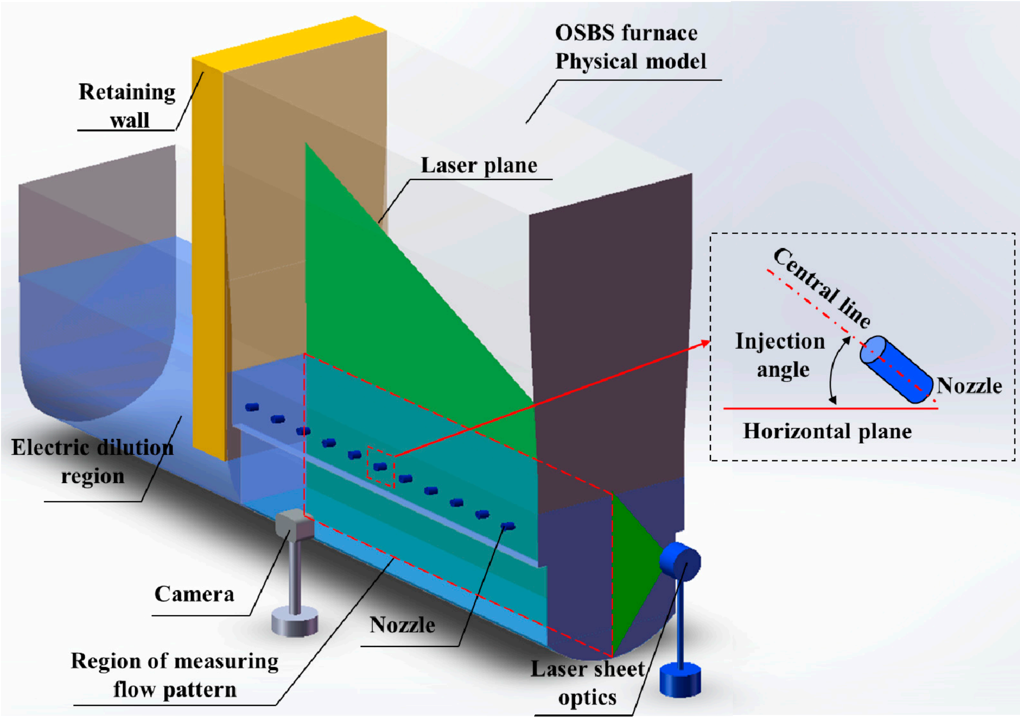

Figure 1. Schematic diagram of the oxygen-rich side-blown bath smelting (OSBS) physical model.

2.2. Experimental Procedure

To begin with, water was added into the OSBS physical model from its top to a height of 300 mm. The oil was then poured slowly into the model and floated on top of the water, with a height of 100 mm. The nozzles were located at the water–oil interface (shown in Figure 1). During the experiment, the compressed air was injected through nozzles at the sides of the OSBS model, thus forming an emulsion. The gas velocity was controlled by the gas flow rate (shown in Table 1), ranging from 44 m/s to 65 m/s. When the two-phase flow was steady, shut off the compressed air. A high-resolution camera (2048 by 2048, FlowSense 4M, Dantec Ltd., Skovlunde, Denmark) was used to take photographs of water–oil emulsification at the side section of the OSBS model.

2.3. Size Analysis of the Emulsified Droplets

In the experiment, the water–oil system was adopted to reproduce the copper slag-matte emulsifying phenomena. The images of emulsion droplets under different operating conditions were analyzed by Image-Pro Plus 6.0 (IPP 6.0, Media Cybernetics, Inc., Rockville, MD, USA) image analysis software to acquire the size distribution of the emulsified droplets. Sauter mean diameter (d_{32}) was utilized to characterize the average size of emulsion droplets in the OSBS system. Sauter mean diameter can be calculated as:

$$d_{32} = \frac{\sum\left(n_{\mathrm{i}} \cdot d_{\mathrm{i}}^{3}\right)}{\sum\left(n_{\mathrm{i}} \cdot d_{\mathrm{i}}^{2}\right)} \tag{4}$$

where d_{i} is the equivalent diameter of a droplet (mm) and n_{i} is the number of drops of diameter d_{i}.

2.4. Measurement of Fluid Pattern

The region in which the flow field was measured was selected in the central region of the OSBS model, as shown in the dashed line region in Figure 1. A 2-D particle image velocimetry (PIV) device (made by Dantec Ltd., Skovlunde, Denmark) was utilized to measure the flow patterns in the OSBS model. The double-pulse Nd:YAG laser system with the maximum laser intensity of 1200 mJ acted as the optical source with 532 nm in the wavelength. The resolution of the camera was 2048 by 2048. The frequency of the laser was set as 10 Hz in the experiments. Besides, polystyrene powder whose density is close to water, 1.03~1.05 g·cm^{-3}, acts as the tracking particle. For every condition, fifty pairs of photos were taken to calculate the average velocity distribution by the PIV image processing system.

3. Results and Discussion

3.1. Effect of Gas Velocity on the Size Distribution of Emulsified Droplets

The typical size distribution of droplets in the emulsified region of a water–oil bath is shown in Figure 2. The increase in gas velocity leads to a decrease in emulsion droplet size. There are many large droplets (over 4 mm in diameter) in the emulsion layer when gas velocity is small. While with the gas velocity gradually increasing to 59 m/s, the percentage of small droplets in the emulsified region also increases. However, the droplet size distribution does not change obviously with a further increment in gas velocity, which is consistent with the conclusions of Khajavi et al. [17]. It also can be found that most droplet sizes are concentrated in the range of 2 mm to 4 mm for all cases.

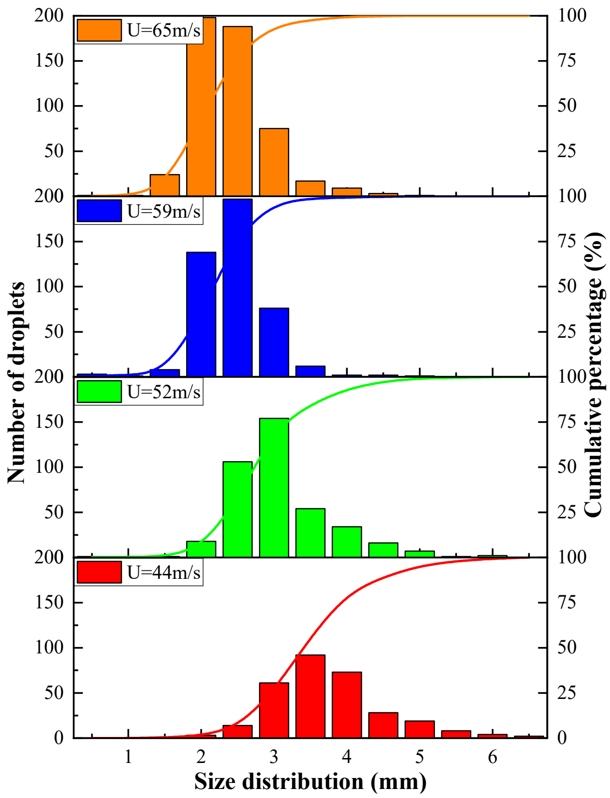

Figure 2. Size distributions of the emulsified droplets against gas velocities.

The control mechanism of emulsion droplet size is discussed to explain the change of droplet size with gas velocity. The deformation, breakage, and size distribution of droplets in turbulence depend on the droplet size, the physical properties of two phases (density, viscosity, interfacial tension, etc.), and the local energy dissipation. Assume an emulsified droplet whose surface is subjected to shear force, turbulent flow, and pressure fluctuation. If the kinetic energy of the droplet is greater than the surface energy generated by droplet breakage, the droplet tends to be broken up. Thus with the increase in gas velocity, the shear stress of the adjacent moving fluid on large droplets will break them into small ones. Whereas smaller droplets are more likely to move around the local vortex rather than being broken up. Smaller droplet has a larger specific surface area, resulting in greater specific surface energy, and therefore requires higher energy input to break it. It is reasonable to consider that for a specific system containing two immiscible liquids and velocity profiles, there is a critical droplet size below which breakage of droplets cannot take place. This is consistent with the results illustrated in Figure 3, indicating that the average droplet size cannot be smaller than 1.5 mm~4.5 mm even at high gas velocities in the water–oil system.

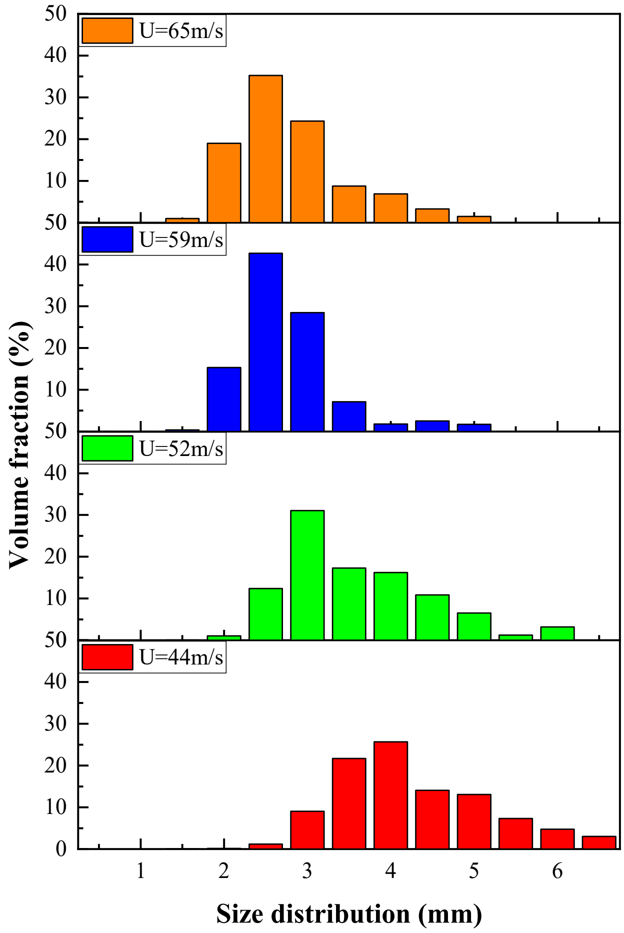

Figure 3. The volume fraction of the emulsified droplets of different sizes.

In addition, the contribution of small droplets to the water–oil interfacial area is small when the gas velocity is small. This is caused by the little volume fraction of small droplets in the emulsion layer. Conversely, the increase in gas velocity can reduce the droplet size and generate more small droplets, which dramatically enlarges the water–oil interfacial area. These can be seen in the volume percentage plots in Figure 3.

3.2. Effect of Injection Angle on the Size Distribution of Emulsified Droplets

The increase in the injection angle (θ) results in the wider distribution of droplet size and a higher proportion of large-size emulsified droplets, as shown in Figure 4. A large injection angle means that the injected gas is more perpendicular to the water–oil interface (shown in Figure 1). This will cause local intensive fluctuations in the water–oil interface. Bubbles can move deeper into the bath and larger droplets of water will be carried up into the emulsified region, which is also found in the investigations of Song et al. [19]. The increase in the volume fraction of the dispersed phase leads to the increment in the effective collision number among droplets, creating large-size emulsified droplets. Moreover, when the injection angle increases, most of the input energy is transferred to the bottom of the bath, while the shear force in the horizontal direction is weakened, which also leads to an increase in droplet diameter. This result is consistent with the conclusions of Koch et al. [18].

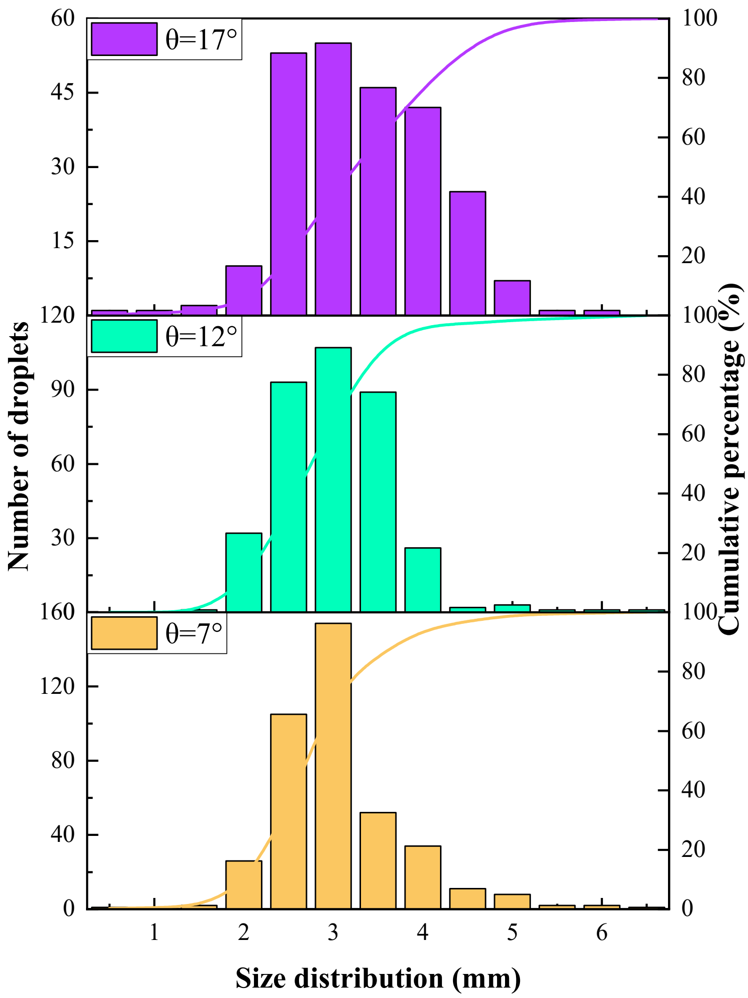

Figure 4. Size distributions of droplets in the emulsified region against injection angles.

From the perspective of industrial practice, the small injection angle is beneficial to strengthen the OSBS process and the optimal value is 7°. The advantage of the OSBS process is to use the kinetic energy of the injected gas to fully stir the molten pool, which is conducive to mixing the reactants well in the emulsion layer and improve the mass transfer rate and the chemical reaction rate. When the injection angle is large, the disturbance effect of the compressed gas in the vertical direction is enhanced, but the mass transfer condition in the horizontal direction is deteriorated, which is not conducive to the full mixing of materials. Moreover, the disturbance in the vertical direction may affect the volume of the quiet area, leading to the enlargement of the emulsion area and contraction of the quiet area, which may worsen the separation performance of slag and metals. Therefore, a small injection angle is beneficial to industrial operations.

3.3. Correlation with Weber Number

The Weber number is the ratio of inertia force to the interfacial tension force, containing the physical properties of fluids (such as density, interfacial tension), flow parameters (e.g., velocity), and characteristic size, which is an important dimensionless number for analyzing two-phase emulsification. The Weber number is expressed as:

$$We = \frac{\rho d U^2}{\sigma} \tag{5}$$

where ρ is the density of injected air, U is the gas velocity at the exit of injector, σ is the interfacial tension of liquids, and d is defined as the diameter of the injector.

Figure 5 illustrates the relationship between Weber number and the Sauter mean diameter of droplets in the emulsified region. An obvious decrease occurs in the average diameter of the emulsified droplet with increasing the Weber number, which indicates that the inertia force of the injected gas dominates the breakage of droplets on the macro scale. Besides, it is also feasible to decrease the droplet size by decreasing the interfacial tension (e.g., adding surface-active agent) under the same velocity profile.

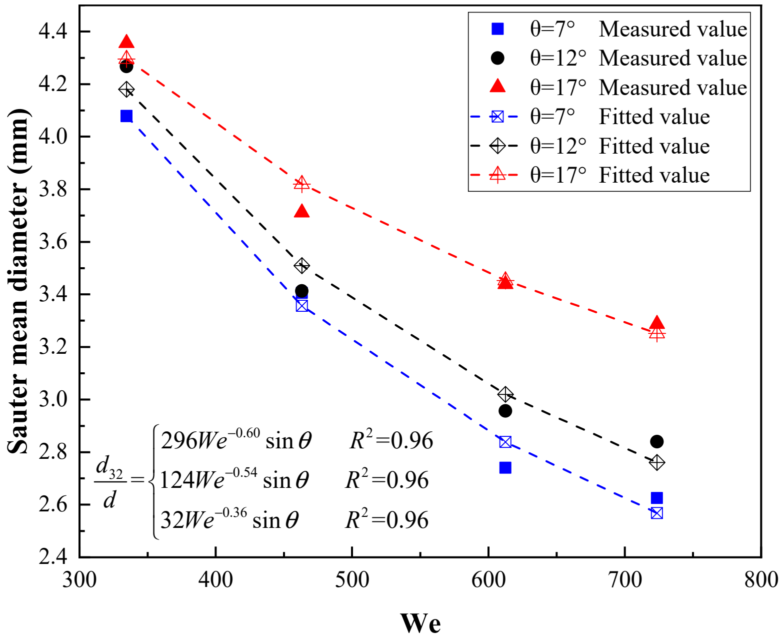

Figure 5. Variations and correlations of d_{32} with Weber number.

Dimensionless correlations of Sauter mean diameter with Weber numbers are also analyzed to predict the droplet size in the emulsified region with the high-strength gas injection. The values obtained from Equation (6) are compared with the experimental data, which yield a good match, as shown in Figure 5. The data shows that the droplet size is negatively correlated with the Weber number. The dimensionless correlations can be used to predict the emulsified droplet size under different operating conditions.

$$\frac{d_{32}}{d} = \begin{cases} 296We^{-0.60}\sin\theta & \theta = 7^\circ \\ 124We^{-0.54}\sin\theta & \theta = 12^\circ \\ 32We^{-0.36}\sin\theta & \theta = 17^\circ \end{cases} \tag{6}$$

3.4. Interfacial Area in Emulsion Region

The interfacial area (A_E) between the emulsified droplets and liquid slag in the emulsified region is a key dynamic parameter for accelerating the copper smelting process and the design of the OSBS reactors. However, the quantitative measurement of A_E in industrial cases is still a challenge because of the complex fluid flow and the limitations of measurement techniques. In this paper, a mathematical method for estimating A_E is proposed and its principle diagram is shown in Figure 6.

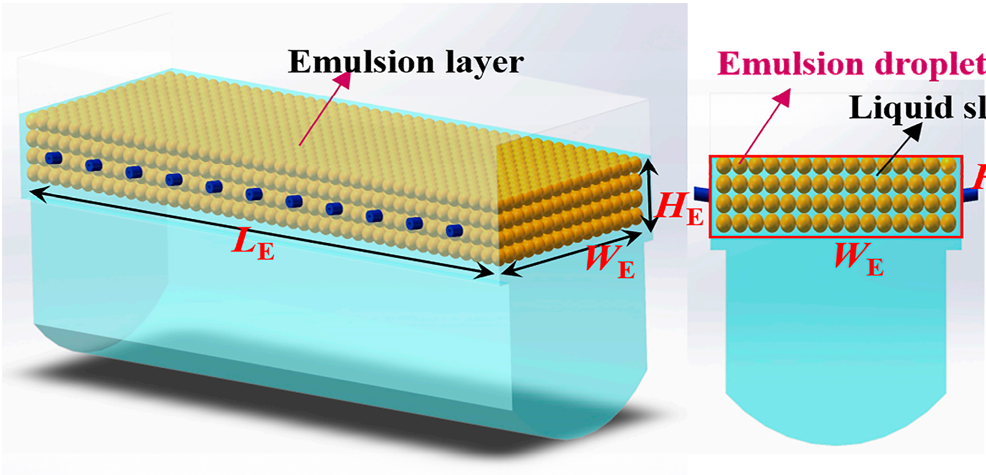

Figure 6. Estimation of the interfacial area of water–oil in the emulsion layer.

The specific interfacial area of the emulsified region is defined as follows:

$$\alpha = \frac{6\varphi}{d_{32}} \tag{7}$$

where α and φ represent the specific interfacial area and the volume fraction of emulsion droplets, respectively.

The interfacial area in the whole emulsion region can be calculated from Sauter mean diameter of droplets d_{32}, the volume fraction φ, and the volume of emulsion layer V, assuming spherical droplets, by the following equation.

$$A_E = \int_V \alpha \mathrm{d}V = \int_V \frac{6\varphi}{d_{32}} \mathrm{d}V \tag{8}$$

The volume of the emulsion layer, V, is determined by the structure of the OSBS reactor and operating conditions. As shown in Figure 6, the shape of the emulsion layer is similar to a cuboid whose length, width, and height are L_E, W_E, and H_E, respectively. L_E and W_E are decided by the structure of the OSBS reactor. Only H_E is the function of operating parameters. Thus, the interfacial area in the emulsion region can be estimated by Equation (9) when the height of the emulsion layer is measured in experiments. Equation (9) can also be applied to reactors of irregular structures to calculate the interfacial area of the dispersed phase.

$$A_E = \int_{H_E} \frac{6\varphi L_E W_E}{d_{32}} \mathrm{d}H_E \tag{9}$$

The volume fraction of emulsion droplets in the emulsion layer, φ, is also determined by operating conditions. Figure 7 shows the emulsion phenomenon in the water–oil system. Spherical and ellipsoidal emulsion droplets of different sizes are closely arranged in the emulsion layer. Therefore, the volume fraction φ is chosen to be one in the next calculation.

It is also significant to estimate the interfacial area of the OSBS process in the industry. According to the similarity principle, the experimental model is consistent with the industrial OSBS furnace structure, and only the size is scaled down. Moreover, the same modified Froude number ensures that the dynamic conditions of the two systems are similar. Therefore, two-phase emulsified phenomena are similar in the OSBS furnaces of different sizes. Thus, the interfacial area of metal-slag in an industrial case can be estimated:

$$A_E^{In} = A_E \cdot S^{-3} \tag{10}$$

where S is the scaling factor (S = 1/8) in this paper.

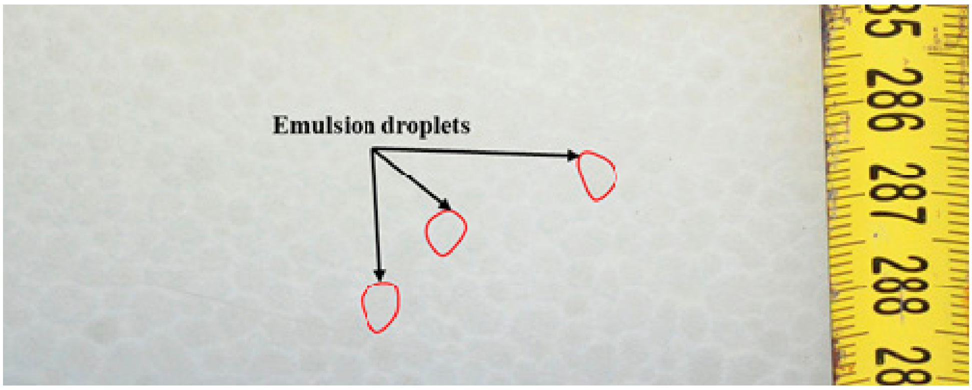

Figure 7. Emulsion droplets in the water–oil physical simulation experiment.

Figure 8 illustrates the interfacial area in both models and practices obtained by Equations (9) and (10). The interfacial area of the emulsified region in the physical model increases dramatically with the increase in gas velocity, reaching 54 m^2. However, with the increment of the injection angle, the interfacial area decreases slightly. It can be seen that gas velocity is the most critical parameter affecting the interfacial area. In addition, when the physical model is scaled up to the industrial scale, the interfacial area could be up to 27,000 m^2. Therefore, from the perspective of chemical reaction kinetics, the formation of emulsion droplets and the control of size distribution are significant factors to accelerate the copper smelting process and improve the efficiency of trapping noble metals.

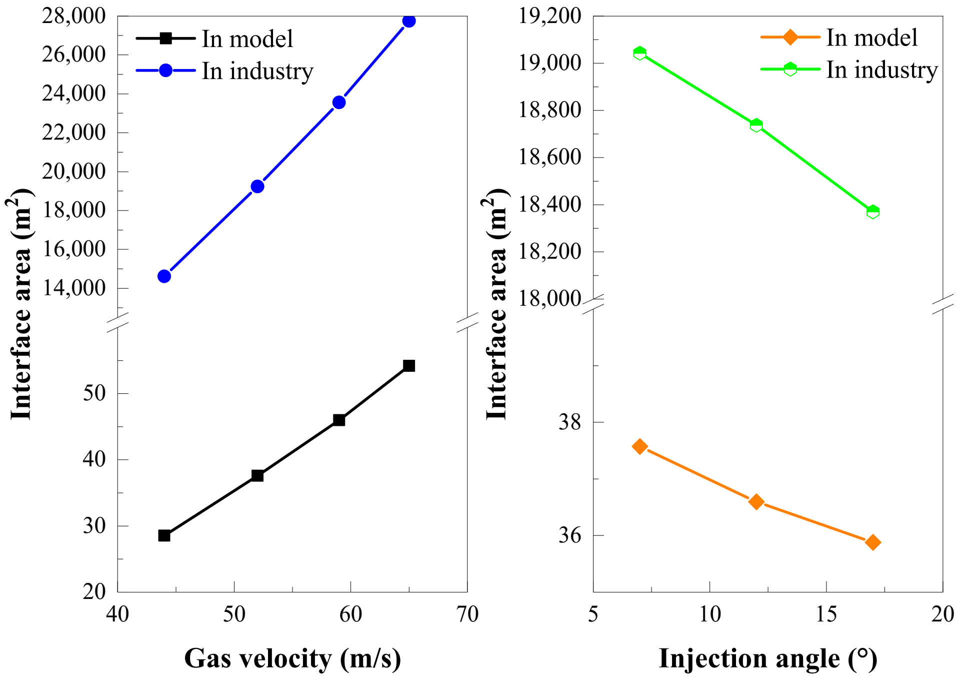

Figure 8. The interfacial area in the emulsion region against gas velocity and injection angle.

3.5. *Effect of Gas Velocity on the Flow Pattern*

The flow patterns shown in Figure 9 can be divided into two zones: The chaotic zone (CZ) and the quiet zone (QZ). The zone with a normalized height greater than 0.6 is defined as the chaotic zone in which the flow patterns are chaotic for all cases. The direction and velocity of the fluid vary greatly, which is caused by high-speed gas. In the chaotic region, the increase of gas velocity improves the mixing performance of fluid, resulting in the smaller emulsified droplets, providing a large interfacial area for chemical reactions. However, an excessively high gas flow rate would enhance the fluctuation and the splashing of fluid in the bath, which is similar to the flow behaviors in the top and bottom-blown smelting process [5,11]. The region below the chaotic zone is defined as the quiet zone where two large circulations dominate the fluid flow. The melt moves down at an average velocity varying from 0.03 m/s to 0.07 m/s. For the industrial OSBS processes, the purpose of the quiet zone is to separate the matte phase from the copper slag phase. Therefore, the appropriate gas velocity (52~59 m/s) can not only optimize the size of the emulsion droplets but also ensure the separating efficiency.

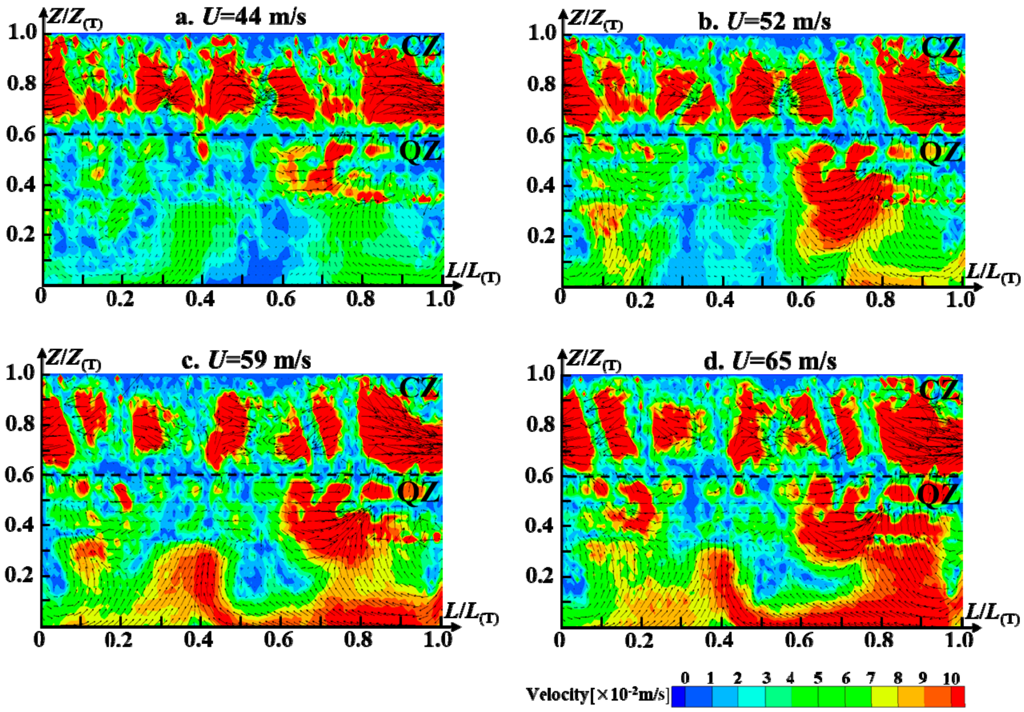

Figure 9. Flow patterns under different gas velocities. (CZ: Chaotic zone; QZ: Quiet zone).

Figure 10 combines the flow patterns in experiments with the industrial OSBS process. The OSBS process can be separated by the retaining wall into two parts, the smelting parts (including the chaotic zone, quiet zone, and matte zone) and the electric dilution part (contains the matte zone and copper slag zone). The compressed gas at a speed of 65 m/s is injected into the chaotic zone, forming the emulsified droplets with an average size of 2.62 mm. In this case, the circulation flow velocity (C 1 and C 2) will be up to 0.1 m/s and the residence time of emulsion droplets in the quiet zone will be shortened, which deteriorates the separating performance between the slag and matte. Therefore, for the same amount of oxygen-rich air, the large-diameter nozzle and the small gas velocity are much better. After the emulsified droplet falling to the matte zone, it will flow to the electric dilution part and will be transformed into the copper slag phase and high-grade matte.

The retaining wall between the smelting part and the electrical dilution part has a good blocking effect on the horizontal movement of the fluid (as shown in Figures 9 and 10), causing the fluid to move towards the quiet zone and preventing the fluid from moving further into the dilution furnace. The proposed height of the retaining wall should be from the top of the smelting furnace to the copper matte layer (shown in Figure 10). It not only prevents the melt from flowing directly into the dilution area but also forces emulsion droplets in the melt to contact with the copper matte layer.

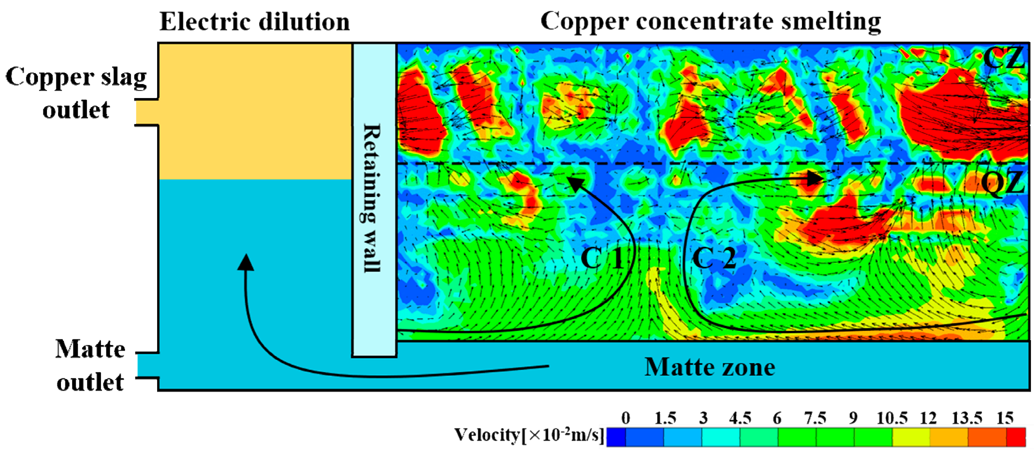

Figure 10. Flow patterns of gas velocity at 65 m/s.

3.6. Effect of Injection Angle on the Flow Pattern

Figure 11 compares the flow states of the melt at three injection angles. The flow patterns turn to be more turbulent with reducing the injection angle. For the quiet zone, there are also two large-scale circulations at the central region of the melt, which dominate the melt flow. With the increase in the injection angle, the energy transferred to the central region decreases gradually. When the angle is 7°, the melt velocity at the junction of the two circulations is about 0.1 m/s. While when the angle increases to 12° and 17°, the fluid flow velocity decreases greatly. Therefore, it is suitable to choose a small injection angle in actual production, which is consistent with the analysis in Section 3.2.

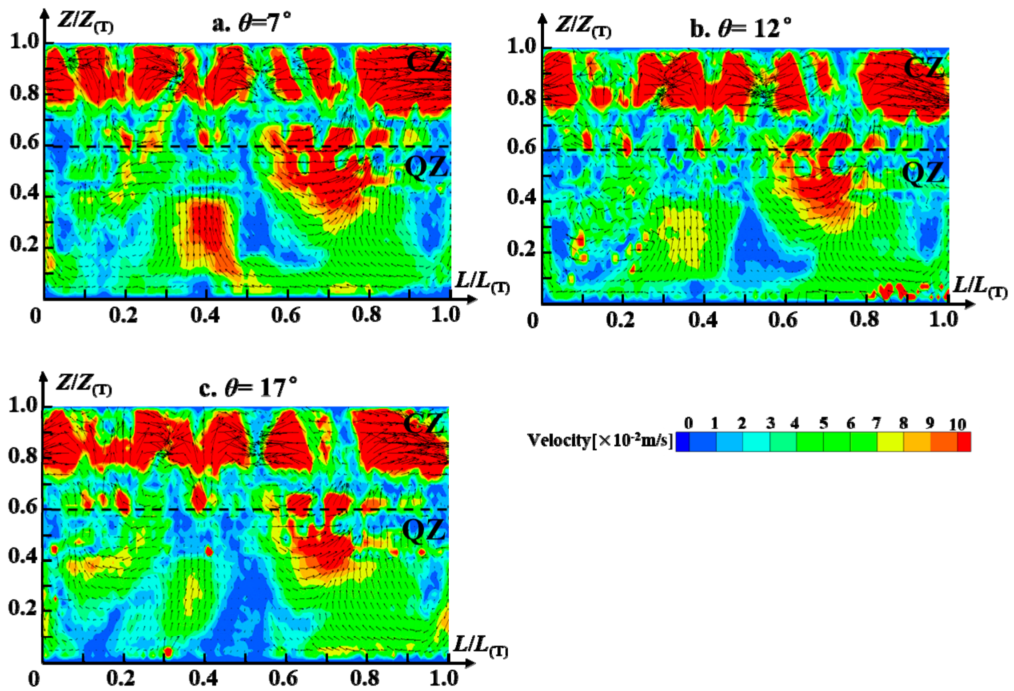

Figure 11. Flow patterns under different injection angles (U = 44 m/s).

4. Conclusions

The emulsification of copper slag-matte and flow behaviors of the melt in the OSBS process were investigated utilizing process simulation. The correlation has been estimated between Sauter mean diameter of droplets in the emulsified region and the Weber number. A mathematical model was also proposed to calculate the interfacial area in the model and industry scales. The small emulsified droplets provide a larger specific surface area, accelerating the reaction rate, and shortening the smelting time.

Gas velocity is an important operational parameter that affects the size distribution of emulsion droplets and the interfacial area. With the increase in gas velocity, the shear force on the emulsified droplets increases, leading to the breakage of droplets and an increase in the interfacial area. The increase of the nozzle angle will result in large-size emulsion droplets and a decrease in the interfacial area. There is a negative correlation between droplet diameter and Weber number, indicating that droplet diameter can be reduced by increasing the gas velocity or decreasing the interfacial tension. The interfacial area in the industrial OSBS furnace is estimated by a mathematical model, up to 27,000 m^2. The flow field plays a decisive role in the flow behavior of emulsion droplets. The flow patterns in the OSBS process can be divided into the chaotic zone and the quiet zone. The increase of gas velocity improves the mixing performance of fluid in the chaotic zone and generates smaller emulsified droplets. However, it will accelerate the velocity of circulation flow in the quiet zone and shorten the separation time between copper slag and matte. Therefore, the appropriate gas velocity (52 m/s~59 m/s) can not only optimize the size of the emulsion droplets but also ensure separating efficiency. A smaller injection angle (7°) is conducive to the refinement of the emulsion droplets.

Author Contributions: Conceptualization, T.Z. and Y.L.; Writing-original draft preparation and methodology, X.L.; Writing-review and editing, D.W.; Investigation and data curation, X.L. and Y.L. All authors have read and agreed to the published version of the manuscript.

Funding: This research was funded by the National Natural Science Foundation of China, U1760120; National Key Research and Development Program of China, 2017YFC0210403.

Conflicts of Interest: The authors declare no conflict of interest.

References

1. Xiong, L.H.; Li, D.L.; Zhang, H.Q.; Han, Y.; Sun, Z.J.; An, T.H. Analysis on supply and demand status and trend analysis of copper resources in the world and China. *Miner. Explor.* **2019**, *10*, 159–164.
2. Chen, L.; Chen, W.; Xiao, H.; Yang, T.Z.; Liu, W.F.; Zhang, D.C. Oxygen-rich side blow bath smelting technology-new development in China. In Proceedings of the 7th International symposium on high-temperature metallurgical processing, Nashville, TN, USA, 14–18 February 2016.
3. Chen, L.; Yang, T.Z.; Bin, S.; Liu, W.F.; Zhang, D.C.; Bin, W.D.; Zhang, L. An efficient reactor for high-lead slag reduction process: Oxygen-rich side blow furnace. *JOM* **2014**, *66*, 1664–1669. [CrossRef]
4. Krishnapisharody, K.; Irons, G.A. A critical review of the modified Froude number in ladle metallurgy. *Metall. Mater. Trans. B* **2013**, *44B*, 1486–1498.
5. Zhao, H.L.; Yin, P.; Zhang, L.F.; Wang, S. Water model experiments of multiphase mixing in the top-blown smelting process of copper concentrate. *Int. J. Min. Met. Mater.* **2016**, *23*, 1369–1376. [CrossRef]
6. Zhao, H.L.; Zhang, L.F.; Yin, P.; Wang, S. Bubble motion and gas-liquid mixing in metallurgical reactor with a top submerged lance. *Int. J. Chem. React. Eng.* **2017**, *15*. [CrossRef]
7. Zhao, H.L.; Lu, T.T.; Liu, F.Q.; Yin, P.; Wang, S. Computational fluid dynamics study on a top-blown smelting process with lance failure in an Isa furnace. *JOM* **2019**, *71*, 1643–1649.
8. Wang, D.X.; Liu, Y.; Zhang, Z.M.; Zhang, T.A.; Li, X.L. PIV measurements on physical models of bottom blown oxygen copper smelting furnace. *Can. Metall. Quart.* **2017**, *56*, 221–231. [CrossRef]
9. Wang, Y.N.; Vanierschot, M.; Cao, L.L.; Cheng, Z.F.; Blanpain, B.; Guo, M.X. Hydrodynamics study of bubbly flow in a top-submerged lance vessel. *Chem. Eng. Sci.* **2018**, *192*, 1091–1104. [CrossRef]
10. Wang, D.X.; Liu, Y.; Zhang, Z.M.; Shao, P.; Zhang, T.A. Dimensional analysis of average diameter of bubbles for bottom blown oxygen copper furnace. *Math. Probl. Eng.* **2016**, *2016*, 4170371. [CrossRef]
11. Shui, L.; Cui, Z.X.; Ma, X.D.; Akbar, R.K.; Nguyen, A.; Zhao, B.J. Mixing phenomena in a bottom blown copper smelter: A water model study. *Metall. Mater. Trans. B* **2015**, *46B*, 1218–1225. [CrossRef]
12. Shui, L.; Cui, Z.X.; Ma, X.D.; Jiang, X.; Chen, M.; Xiang, Y.; Zhao, B.J. A water model study on mixing behavior of the two-layered bath in bottom blown copper smelting furnace. *JOM* **2018**, *70*, 2065–2070. [CrossRef]
13. Sahai, Y. Fluid dynamics in channel reactors stirred by submerged gas injection. *Metall. Mater. Trans. B* **1988**, *19B*, 603–612. [CrossRef]

14. Jiang, X.; Cui, Z.X.; Chen, M.; Zhao, B.J. Mixing behaviors in the horizontal bath smelting furnaces. *Metall. Mater. Trans. B* **2018**, *50B*, 173–180. [CrossRef]
15. Kapusta, J.P.T. Submerged gas jet penetration: A study of bubbling versus jetting and side versus bottom blowing in copper bath smelting. *JOM* **2017**, *69*, 970–979.
16. Brämming, M.; Engström, F.; Samuelsson, C.; Björkman, B. Characterization of slag-metal emulsion and its impact on foaming behavior and slopping in the LD process. *Steel Res. Int.* **2019**, *90*, 1–11. [CrossRef]
17. Khajavi, L.T.; Barati, M. Cold model study of emulsification behavior in bottom blown metallurgical baths covered with thick slag. *ISIJ Int.* **2010**, *50*, 654–662. [CrossRef]
18. Koch, K.; Falkus, J.; Brukhaus, R. Hot model experiments of the metal bath spraying effect during the decarburization of Fe-C melts through oxygen top blowing. *Steel Res.* **1993**, *64*, 15–21. [CrossRef]
19. Song, D.Y.; Maruoka, N.; Maeyama, T.; Shibata, H.; Kitamura, S.Y. Influence of bottom bubbling condition on metal emulsion formation in lead-salt system. *ISIJ Int.* **2010**, *50*, 1539–1545. [CrossRef]
20. Martín, M.; Rendueles, M.; Díaz, M. Emulsion analysis in a gas/liquid/liquid reactor with top blowing. *Can. J. Chem. Eng.* **2014**, *82*, 249–255. [CrossRef]
21. Lin, Z.H.; Guthrie, R.I.L. Modeling of metallurgical emulsions. *Metall. Mater. Trans. B* **1994**, *25B*, 855–864. [CrossRef]
22. Akdogan, G.; Eric, R.H. Physical modelling of slag-metal dispersion. *J. S. Afr. I. Min. Metall.* **2004**, *104*, 671–678.
23. Spooner, S.; Warnett, A.M.; Bhagat, R.; Williams, M.A.; Sridhar, S. Calculating the macroscopic dynamics of gas/metal/slag emulsion during steelmaking. *ISIJ Int.* **2016**, *56*, 2171–2180. [CrossRef]
24. Subaguo; Brooks, G.A.; Coley, K.S.; Irons, G.A. Generation of droplets in slag–metal emulsions through top gas blowing. *ISIJ Int.* **2003**, *43*, 983–989. [CrossRef]
25. Brooks, G.; Pan, Y.H.; Subagyo; Coley, K. Modeling of trajectory and residence time of metal droplets in slag-metal-gas emulsions in oxygen steelmaking. *Metall. Mater. Trans. B* **2005**, *36B*, 525–535. [CrossRef]
26. Deo, B.; Karamcheti, A.; Paul, A.; Singh, P.; Chhabra, R.P. Characterization of slag-metal droplets-gas emulsion in oxygen steelmaking converters. *ISIJ Int.* **1996**, *36*, 658–666. [CrossRef]
27. Zlokarnik, M. *Scale-Up in Chemical Engineering*, 2nd ed.; Wiley-VCH: Weinheim, Germany, 2006; pp. 25–30.
28. Xu, H.L.; Wen, G.H.; Tang, P. Similarity transformation of gas blowing rate in physical simulation of continuous casting models. *J. Univ. Sci. Technol. B* **2010**, *32*, 843–848.
29. Han, J.; Wang, X.D.; Ba, D.C. Physical simulation on circulating flow rate and mixing characteristics in RH vacuum refining process. *J. Northeast. Univ.* **2013**, *34*, 975–979.
30. Themelis, N.J.; Tarasoff, P.; Szekely, J. Gas-liquid momentum transfer in a copper converter. *Trans. Am. I. Min. Metall. Pet. Eng.* **1969**, *245*, 2425–2433.